Superconductor Science and Technology

PAPER

Enhancement of the lower critical field in FeSe-coated Nb structures for superconducting radio-frequency applications

To cite this article: Zefeng Lin *et al* 2021 *Supercond. Sci. Technol.* **34** 015001

IOP Publishing Superconductor Science and Technology
Supercond. Sci. Technol. **34** (2021) 015001 (5pp) https://doi.org/10.1088/1361-6668/abc568

Enhancement of the lower critical field in FeSe-coated Nb structures for superconducting radio-frequency applications

Zefeng Lin[1,2], Mingyang Qin[1,2], Dong Li[1,2], Peipei Shen[1,2], Liping Zhang[3], Zhongpei Feng[4], Peng Sha[5], Jun Miao[3], Jie Yuan[1,6], Xiaoli Dong[1,2,4], Chao Dong[5], Qing Qin[7] and Kui Jin[1,4,6]

[1] Beijing National Laboratory for Condensed Matter Physics, Institute of Physics, Chinese Academy of Sciences, Beijing 100190, People's Republic of China
[2] School of Physical Sciences, University of Chinese Academy of Sciences, Beijing 100049, People's Republic of China
[3] School of Materials Science and Engineering, University of Science and Technology Beijing, Beijing 100083, People's Republic of China
[4] Songshan Lake Materials Laboratory, Dongguan, Guangdong 523808, People's Republic of China
[5] Institute of High Energy Physics, Chinese Academy of Sciences, Beijing 100049, People's Republic of China
[6] Key Laboratory for Vacuum Physics, University of Chinese Academy of Sciences, Beijing 100049, People's Republic of China
[7] School of Physics, Peking University, Beijing 100871, People's Republic of China

E-mail: dongchao@ihep.ac.cn

Received 19 March 2020, revised 1 October 2020
Accepted for publication 28 October 2020
Published 13 November 2020

Abstract

Bulk Nb superconducting radio-frequency (SRF) cavities are widely used in accelerators, and their accelerating gradient and general performance are limited by the superheating field (B_{sh}). To push the theoretical limit of the B_{sh}, new multilayer structures are required. We fabricated FeSe-coated Nb films using pulsed laser deposition, performed structural characterizations, and measured the transport and magnetic properties for this superconductor-superconductor bilayer structure with smooth surface. Additionally, the measured B_{c1} of FeSe-coated Nb film is greatly enhanced, while the B_{sh} of the FeSe layer is expected to be higher than that of bulk Nb, yet the superconducting transition temperature (T_c) is less than 5 K. This work presents the first fabrication of a new coating layer: FeSe deposited on Nb, showing the possibility of using iron-based materials for multilayer structures in SRF cavities.

Keywords: iron-based superconductors, SS' structures, the lower critical field, SRF

(Some figures may appear in colour only in the online journal)

1. Introduction

At present, bulk Nb is the best candidate for SRF cavity applications in different types of accelerators [1–5]. It benefits from having the highest critical temperature ($T_c = 9.25$ K) and the highest lower critical field (B_{c1}) among all the pure metals; it is also relatively simple to fabricate and process. There are two important indicators of superconducting cavity performance: accelerating gradient (E_{acc}) and quality factor (Q_0). Q_0 represents the cavity efficiency; the higher the Q_0, the lower the power dissipated in the walls of the cavity. E_{acc} determines the effective length of the accelerator required to raise the energy

of a particle beam to a given value; it is proportional to the peak magnetic field parallel to the cavity surface (B_{pk}). For a Tesla-shape cavity [6], $B_{pk}/E_{acc} = 4.18$ mT (MV m^{-1})$^{-1}$. Therefore, Nb cavities are limited by B_{pk}; once B_{pk} reaches the superheating field (B_{sh}), which defines the theoretical limit of the SRF breakdown, flux will penetrate into the superconductor in the form of vortices and produce dissipation [7, 8].

The RF performance of Nb cavities, which has been improved significantly over time, is now approaching the intrinsic material limit ($B_{(sh,Nb)}$ (0 K) $\approx$ 240 mT, corresponding to $E_{acc} = 57$ MV m^{-1}) [9]. For example, the best E_{acc} of the Tesla type 1.3 GHz 9-cell cavities in vertical tests is now more than 40 MV m^{-1} ($B_{pk} > 165$ mT) [10–12] in some laboratories. Once the magnetic field limit is reached, there will only be a very small margin for improvement. The urgent need for higher gradients in future accelerators has renewed interest in alternatives. Reference [13] gives an overview of materials being considered, and one can find the potential candidates for SRF applications. Among these candidates, Nb_3Sn-coated cavities have already succeeded in vertical tests with a record of accelerating gradient exceeding 22 MV m^{-1} [14], whose corresponding quench field B_q was still less than half of the B_{sh} [15].

According to [13], iron-based superconductors benefit from a higher T_c and potentially a higher B_{sh} than Nb. To obtain a higher B_{sh}, a multilayer nanoscale coating inside of the Nb cavity may shift the RF breakdown field to the level of the B_{sh} of the coating materials [16, 17]. That is, the coating film will partially shield the bulk Nb from the applied RF magnetic field, and the multilayer structure would withstand a higher field than the bulk Nb. Using iron-based superconductor coatings in multilayer structures has not yet been experimentally reported, to our knowledge. This paper focuses on the simplest case of a Nb thin film coated with a single layer of FeSe, which has a comparatively simple chemical composition in the iron-based family, and shows the potential to have a higher B_{sh} than the state-of-the-art bulk Nb cavities. In the following sections, it is needed to compare the critical field of FeSe, Nb and FeSe-coated Nb. Considering that FeSe with different T_c from 2 K to 14 K can be prepared on CaF_2 substrates in [18], and the substrate variable should be unified to ensure the consistency of the magnetic background signal, we chose CaF_2 as the substrate.

2. Experiments

The target, with a nominal composition of $FeSe_{0.98}$, was prepared by solid-state reaction (see details in [18]). The FeSe thin films were fabricated by pulsed laser deposition (PLD) on (00l)-oriented single-crystal CaF_2 substrates with a 115 nm thick Nb buffer layer. A 350 mJ KrF excimer laser ($\lambda = 248$ nm) was used for film deposition, with a repetition rate of 4 Hz. The base pressure was 10^{-7} Torr and the substrate temperature was 350 °C. The FeSe film was 5 × 5 mm^2 in size and around 130 nm in thickness. The structural characterizations were performed in a 9 kW Rigaku SmartLab x-ray diffractometer (XRD) with two Ge (220) single crystals. The

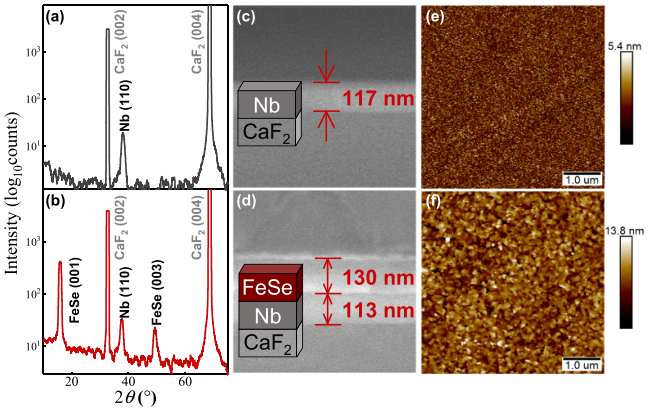

Figure 1. θ–2θ scans of Nb/CaF_2 (a) and FeSe/Nb/CaF_2 (b). SEM cross-sectional images of Nb/CaF_2 (c) and FeSe/Nb/CaF_2 (d). AFM images (5 × 5 μm^2) of Nb/CaF_2 (e) and FeSe/Nb/CaF_2 (f). The root-mean-square roughness of Nb/CaF_2 and FeSe/Nb/CaF_2 are approximately 0.773 nm and 1.89 nm, respectively.

scanning electron microscopy (SEM) measurements were performed using a Hitachi SU5000. The transport properties were measured using the 4-probe method in the Physical Property Measurement System (PPMS-9T). The DC magnetic moment (m) was measured in the Magnetic Property Measurement System (MPMS XL-1) with the magnetic field parallel to the film surface.

3. Results and discussion

3.1. Structural characterizations

Figure 1(a) illustrates the out-of-plane θ–2θ XRD scan of a Nb film grown on a (00l) CaF_2 substrate (Nb/CaF_2). Figure 1(b) shows the same scan for an FeSe film grown on Nb-coated CaF_2 (FeSe/Nb/CaF_2). For both Nb layers, the peaks at $2\theta \approx 38.5$ represent the (110) reflection. For FeSe/Nb/CaF_2, only the (00l) diffraction peaks from the FeSe layer are observed, indicating that the out-of-plane alignment is good. Figure 1(c) is the SEM cross-sectional image of Nb/CaF_2, which shows a uniform Nb layer thickness of about 117 nm. Figure 1(d) exhibits the clear FeSe/Nb bilayer with a FeSe layer of about 130 nm. This indicates that we can control the thicknesses of FeSe and Nb layers, and maintain a sharp interface between them. The atomic force microscopy (AFM) image of Nb/CaF_2 (figure 1(e)) shows that the root-mean-square roughness is around 0.773 nm, confirming that the Nb layer is as flat as the commercial CaF_2 substrate. And the root-mean-square roughness of FeSe/Nb/CaF_2 is 1.89 nm (figure 1(f)), which is comparable with that of Nb/CaF_2. Both uniform thickness and small roughness benefit the Bean-Livingston barrier, which can prevent the penetration of the vortex and induce a higher B_{sh}.

3.2. Verification of SS' structure

Figures 2(a) and (b) show the temperature-dependent resistances of Nb/CaF_2 and FeSe/Nb/CaF_2 under different magnetic

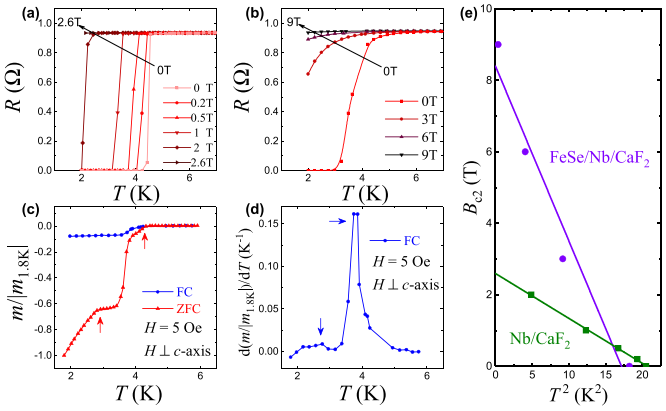

Figure 2. Temperature dependences of the following: resistance under various magnetic fields for Nb/CaF_2 (a) and $FeSe/Nb/CaF_2$ (b); DC normalized magnetic moments, measured in zero-field-cooling (ZFC) and field-cooling (FC) modes (c); and dm/dT (d) extracted from DC normalized magnetic moments in FC mode (FC curve in (c)); the arrows indicate superconducting transitions. $B_{c2}(T)$ obtained from 90% transition is plotted as a function of T^2(e). The two lines were fitted using the formula $B_{c2}(T) = B_{c2}(0)\left[1-(T/T_c)^2\right]$.

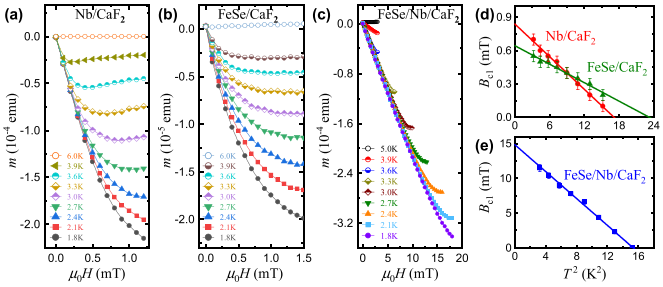

Figure 3. $m(H)$ curves of Nb/CaF_2 (a), $FeSe/CaF_2$ (b) and $FeSe/Nb/CaF_2$ (c) at various temperatures for H parallel to the film surface. T^2 dependence of B_{c1} for Nb/CaF_2 (red line), $FeSe/CaF_2$ (olive line) (d), and $FeSe/Nb/CaF_2$ (blue line) (e). The three lines were fitted using the formula $B_{c1}(T) = B_{c1}(0)\left[1-(T/T_c)^2\right]$.

fields perpendicular to the film surface. The zero-resistivity transition temperature (T_c) of Nb/CaF_2 is about 4.24 K, and the resistive transition is very sharp under zero magnetic field. The superconductivity is completely suppressed for magnetic fields reaching 2.6 T. However, for an FeSe film deposited on the Nb surface, the case is rather different. The superconducting transition of $FeSe/Nb/CaF_2$ under zero magnetic field is much smoother than that of Nb/CaF_2 (figure 2(b)). The superconducting onset temperature (T_c^{onset}) and the T_c of $FeSe/Nb/CaF_2$ is about 4.43 K and 2.97 K, respectively. The T^2 dependence of the upper critical field B_{c2} for Nb/CaF_2 and $FeSe/Nb/CaF_2$, estimated at 90% of the resistance transition relative to the normal state resistance, are shown in figure 2(e). The $B_{c2}(T)$ lines of Nb/CaF_2 and $FeSe/Nb/CaF_2$ were fitted using the formula $B_{c2}(T) = B_{c2}(0)\left[1-(T/T_c)^2\right]$ [19]. It was obvious that the $B_{c2}(0)$ of $FeSe/Nb/CaF_2$ was considerably larger than that of Nb/CaF_2, indicating that the FeSe layer contributes to the superconductivity of $FeSe/Nb/CaF_2$. To verify the existence of the superconductor-superconductor (SS') bilayer, the DC susceptibilities of the $FeSe/Nb/CaF_2$ heterostructure were investigated (figures 2) and (d)). Two superconducting transitions in the DC susceptibility in zero-field-cooling (ZFC) mode (figure 2(c)), occurring at 4.28 K and 2.90 K, suggest the existence of two superconducting states. Two distinct peaks in dm/dT (T) curve extracted from figure 2(c) in field-cooling (FC) mode were observed (see figure 2(d)), which arose from the contributions of the FeSe and Nb layers, rather than inhomogeneous superconductivity resulting from either layer.

3.3. *Analysis of the lower critical field*

Samples for MPMS measurements were cut to less than 5×5 mm^2 and aligned parallel to the magnetic field, i.e. 'in-plane' geometry, which precisely simulates magnetic field direction in a cavity [20]. To compare the B_{c1} values of Nb/CaF_2, $FeSe/CaF_2$, and $FeSe/Nb/CaF_2$, the in-plane $m(H)$ curves under low fields at various temperatures are plotted in figures 3(a)–(c). All curves exhibit linear behavior for low fields and then deviate from linearity at different field values for different temperatures; the B_{c1} value is determined from where the deviation occurs. The T^2 dependence of $B_{c1}(T)$ are fitted by the formula $B_{c1}(T) = B_{c1}(0)\left[1-(T/T_c)^2\right]$ [19], as shown in figures 3(d) and (e). By extrapolating the B_{c1} to zero, the T_c values of Nb/CaF_2, $FeSe/CaF_2$, and $FeSe/Nb/CaF_2$ are given 4.12 K, 4.80 K and 3.90 K, respectively. In addition, by extrapolating the T^2 to zero, the $B_{c1}(0)$ values of Nb/CaF_2, $FeSe/CaF_2$, and $FeSe/Nb/CaF_2$ are 0.83 mT, 0.64 mT and 14.8 mT, respectively. It is clear that the $B_{c1}(T)$ of $FeSe/Nb/CaF_2$ is greatly enhanced, particularly $B_{c1}(0)$ for $FeSe/Nb/CaF_2$ reaches above ten times higher than either of Nb/CaF_2 and $FeSe/CaF_2$, even though only one side of Nb film is covered with FeSe layer. Therefore, the combination of FeSe and Nb layers can effectively offer the higher $B_{c1}(T)$. A similar phenomenon was also observed in NbN deposited on a Nb layer [21]. They found that the B_{c1} of a multilayer is enhanced 5.3 times than the single layers when the field is parallel to the surface. Note that the first flux will enter the $FeSe/Nb/CaF_2$ structure from either the FeSe layer or Nb layer, in the configuration where the magnetic field is parallel to the surface of $FeSe/Nb/CaF_2$, which means that the $B_{c1}(0)$ of the FeSe layer is not less than 14.8 mT. When the Ginzburg–Landau parameter $\kappa \gg 1/\sqrt{2}$, we have [19, 22]

$$B_c/B_{c1} = \sqrt{2}\kappa/\ln\kappa \tag{1}$$

$$B_{sh}/B_c \approx \sqrt{2}\cdot\left(\sqrt{10}/6 + 0.3852\kappa^{-1/2}\right) \tag{2}$$

where B_c is the thermodynamic critical field. Assuming that κ is 80 for FeSe in [23] or 72 in [24], the $B_{sh}(0)$ of the FeSe layer is calculated to be about 312 mT or 288 mT, above 20% higher than that of bulk Nb. Taking into account the upper critical field anisotropy of 2, κ can be estimated conservatively to be about 47 using the measured $B_{c2}(0)$ and $B_{c1}(0)$ values and then the

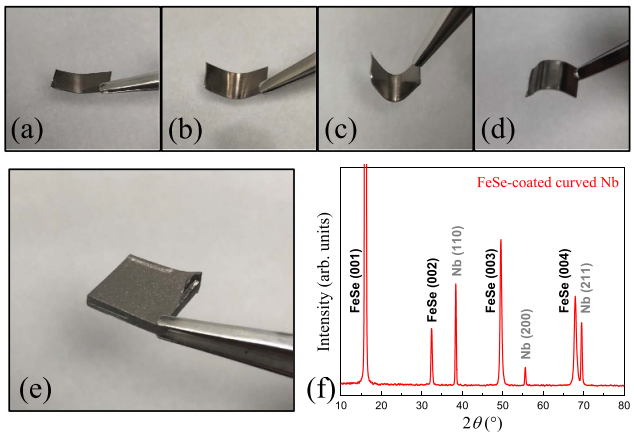

Figure 4. The FeSe-coated Nb foil was bent to inward angles 160°, 120°, 60° and outward angle 90°, in (a)–(d), respectively. A diagram (e) and θ–2θ scans (f) of FeSe-coated curved bulk Nb.

$B_{sh}(0)$ is 210 mT, which is close to that of bulk Nb. Note that there is still much room for improvement in critical parameters of FeSe layer, such as T_c, B_{c2} and B_{c1}. In particular, higher B_{c1} can be achieved with the film thickness much smaller than the penetration depth λ, in a configuration where the magnetic field is parallel to the surface of the film [17]. Thus, the more dramatic improvement in B_{sh} in the FeSe/Nb structure could be expected to achieve.

3.4. Curved surface stability

The curved surface stability, in addition to the B_{sh}, affects whether a candidate is suitable for multilayers for RF field screening applications. Figures 4(a)–(e) exhibit photos of FeSe-coated Nb foil and FeSe-coated curved bulk Nb, respectively. Figures 4(a)–(d) show that the FeSe layer remained tightly attached to the surface, even when bent inward or outward to varying degrees, repeatedly, showing the FeSe layer's high toughness. Furthermore, FeSe can be fabricated on a 10×10 mm^2 curved Nb cut from a cavity (see figure 4(e)). In figure 4(f), the FeSe layer still exhibits a single preferred (00l) crystal orientation on this polycrystalline Nb substrate with a micron-scale rough surface. Both samples manifestly show that FeSe can satisfy the basic coating conditions as an alternative material in SRF cavities. Similarly, reference [25] reported to succeeded in fabricating c-axis preferred textured Fe(Se, Te) superconducting films with $T_{c0} \sim 5$ K on Al_2O_3 buffered metal substrates. Moreover, the Fe(Se, Te) film on the metal can also achieve good bending. All these results help to lay a foundation toward practical applications of iron-based superconductor coated metal.

4. Conclusion

We can make several useful observations from the above experimental results. First, this work confirms for the first time that it is experimentally possible to deposit a crystalline and superconducting FeSe layer with (00l)-oriented on Nb. Second, utilizing m–H measurements, one can infer that the B_{c1} of FeSe/Nb/CaF_2 is greatly enhanced. Third, an FeSe film can be fabricated on curved bulk Nb and withstand multi-angle bending. These observations all support the potential application of FeSe in multilayer structures for SRF cavities. However, further work is still required. For example, it is necessary to more precisely determine B_{c1} when the first flux enters FeSe/Nb/CaF_2 solely from the surface of the FeSe layer. On the other hand, the superconductor-insulator-superconductor (SIS') multilayer structure proposed by Gurevich [13, 17] would prevent Josephson coupling between coating layers and bulk Nb, and achieve better shielding than a single FeSe layer. Experimentally, multilayers $(NbN/MgO)_n$ [21, 26, 27] and NbN/SiO_2 [28] both showed a dramatic enhancement of B_{c1}. Thus, further study is needed to fabricate an SIS' structure using an FeSe layer.

Iron-based superconductors are rarely studied for SRF applications, yet they have higher superconducting critical parameters than most conventional superconductors, such as critical magnetic field and critical current density [29]. In this work, we chose FeSe, the material with the simplest structure in the iron-based family, to coat the Nb film. Structural characterizations, toughness tests, and measurements of the transport and magnetic properties were performed on this SS' structure. The results demonstrate FeSe's suitability for application in superconducting cavities, due to its crystallinity, enhanced B_{c1}, high B_{sh} and good flexibility. We are eager for this work to allow more researchers to focus on neglected alternative materials, especially iron-based superconductors with higher critical parameters.

Acknowledgments

This work was supported by the Strategic Priority Research Program of Chinese Academy of Sciences (Grant No. XDB25000000), Key Research Program of Frontier Sciences, CAS (Grant Nos. QYZDJ-SSW-SLH001 and QYZDB-SSW-SLH008), the National Key Basic Research Program of China (Grant Nos. 2016YFA0300301, 2017YFA0302902, 2017YFA0303003 and 2018YFB0704102), the National Natural Science Foundation of China (Grant Nos. 11674374, 11811530147, 11834016, 11927808, 11961141008), CAS Interdisciplinary Innovation Team, Beijing Natural Science Foundation (Grant No. Z190008).

ORCID iDs

Zefeng Lin https://orcid.org/0000-0002-5407-9696
Dong Li https://orcid.org/0000-0002-0823-195X
Peng Sha https://orcid.org/0000-0003-2545-7974
Jun Miao https://orcid.org/0000-0002-6924-0737
Xiaoli Dong https://orcid.org/0000-0002-6268-2049
Kui Jin https://orcid.org/0000-0003-2208-8501

References

[1] Brüning O S, Collier P, Lebrun P, Myers S, Ostojic R, Poole J and Proudlock P 2004 *LHC Design Report* (CERN: Geneva)
[2] Altarelli M *et al* 2006 *XFEL: The European X-Ray Free-Electron Laser: Technical Design Report* (Hamburg: DESY)
[3] Mason T E *et al* 2006 *Physica* B **385–6** 955–60
[4] Peggs S 2012 *European Spallation source: Conceptual design report* (Lund: ESS)
[5] Galayda J N 2015 *LCLS-II Final Design Report* (Menlo Park: SLAC)
[6] Juntong N and Jones R M 2009 e-print (arXiv: 0910.1305) (physics. acc-ph)
[7] Matricon J and Saint-James D 1967 *Phys. Lett.* A **24** 241–2
[8] Catelani G and Sethna J P 2008 *Phys. Rev.* B **78** 224509
[9] Kubo T 2017 *Supercond. Sci. Technol.* **30** 023001
[10] Singer W *et al* 2013 *Phys. Rev. Spec. Top. Accel. Beams* **16** 012003
[11] Romanenko A, Grassellino A, Barkov F and Ozelis J P 2013 *Phys. Rev. Spec. Top. Accel. Beams* **16** 012001
[12] Grassellino A *et al* 2017 *Supercond. Sci. Technol.* **30** 094004
[13] Gurevich A 2017 *Supercond. Sci. Technol.* **30** 034004
[14] Posen S, Tennis B, Lee J Y, Melnychuk O S, Pischalnikov Y M and Sergatskov D A 2019 *19th Int. Conf. on RF Superconductivity*
[15] Posen S, Valles N and Liepe M 2015 *Phys. Rev. Lett.* **115** 047001
[16] Kubo T, Iwashita Y and Saeki T 2014 *Appl. Phys. Lett.* **104** 032603
[17] Gurevich A 2006 *Appl. Phys. Lett.* **88** 012511
[18] Feng Z *et al* 2018 *Sci. Rep.* **8** 4039
[19] Tinkham M 1996 *Introduction to Superconductivity* (New York: McGraw-Hill)
[20] Beringer D B, Clavero C, Tan T, Xi X X, Roach W M and Lukaszew R A 2013 *IEEE Trans. Appl. Supercond.* **23** 7500604
[21] Antoine C Z, Berry S, Bouat S, Jacquot J F, Villegier J C, Lamura G and Gurevich A 2010 *Phys. Rev. Spec. Top. Accel. Beams* **13** 121001
[22] Liarte D B, Transtrum M K and Sethna J P 2016 *Phys. Rev.* B **94** 144504
[23] Kasahara S *et al* 2014 *Proc. Natl Acad. Sci. USA* **111** 16309–13
[24] Yang H, Chen G, Zhu X, Xing J and Wen H-H 2017 *Phys. Rev.* B **96** 064501
[25] Huang J, Chen L, Jian J, Khatkhatay F, Jacob C and Wang H 2015 *J. Alloys Compd.* **647** 380–5
[26] Antoine C Z, Villegier J C and Martinet G 2013 *Appl. Phys. Lett.* **102** 102603
[27] Antoine C Z, Aburas M, Four A, Weiss F, Iwashita Y, Hayano H, Kato S, Kubo T and Saeki T 2019 *Supercond. Sci. Technol.* **32** 085005
[28] Ito H, Hayano H, Kubo T, Saeki T, Katayama R, Iwashita Y, Tongu H, Ito R, Nagata T and Antoine C Z 2019 e-print (arXiv: 1907.03410) (physics. acc-ph)
[29] Hosono H, Yamamoto A, Hiramatsu H and Ma Y 2018 *Mater. Today* **21** 278–302